THE AMAZON RIVER BREEZE AND THE LOCAL BOUNDARY LAYER: II. LINEAR ANALYSIS AND MODELLING

AMAURI PEREIRA DE OLIVEIRA

Departmento de Ciencias Atmosféricas, Instituto Astronômico e Geofísco, Universidade de São Paulo, Brazil

and

DAVID R. FITZJARRALD

Atmospheric Sciences Research Center, State University of New York, Albany 12205, USA

(Received in final form 7 April, 1993)

Abstract. Observed boundary-layer circulations close to the confluence of the Negro and Solimões rivers near Manaus in the Brazilian equatorial Amazon forest were presented in Part I. These are shown through linear analysis and second-order turbulence modelling to be aspects of a river breeze superimposed on the basic flow. Linear analysis is presented to estimate the spatial structure and intensity of a breeze induced by a river with width and thermal contrast similar to that observed in the central Amazon. It is found that observed thermal contrasts are sufficient to produce a river breeze that can be perceived more than 20 km inland daily. A one-dimensional second-order closure model is used to show that observed nocturnal low-level wind maxima and diurnal surface wind rotation are aspects of a river breeze interacting with the seasonally-varying mean flow. At night, partial decoupling of the surface from the lower atmosphere allows the land breeze to be expressed as a low-level wind maximum. During the day, convective mixing communicates upper level winds to the surface during rapid morning boundary-layer growth. Rotation of the surface wind follows as the river breeze circulation is then superimposed.

1. Introduction

Analysis of data from the Amazon Boundary Layer Experiments (ABLE-2a and ABLE-2b, Harriss *et al.*, 1988, 1990) indicated the presence of several features of the PBL in the central Amazon near the large rivers (Oliveira and Fitzjarrald, 1992, Part I, hereafter OF): (1) Circulations confined to the first 500 m exhibiting nocturnal flow toward the river reversing in the daytime; (2) A diurnal oscillation in the horizontal pressure and temperature gradients as well as in the divergence near the surface; (3) Rotation of the surface wind direction through the day, with the average wind vector describing approximately elliptical trajectories; (4) Boundary-layer wind maxima formed predominantly during the transition period (0600–0900 LT) in the 1985 dry season and during the night in the 1987 wet season. Two classes of low level wind maxima were identified. The first, observed at the first 200–400 m above the surface is characterized by low level wind maxima of 2–6 m/s with significant wind directional shear, and a second class observed within the first 400–600 m, with intensity 10–15 m/s, exhibiting little directional shear.

Boundary-Layer Meteorology **67**: 75–96, 1994.

Since dry-season aircraft measurements indicated a daytime thermal contrast between the Negro River and the surrounding forest to be approximately +6 °C during the day and −3 °C at night, the existence of a river breeze circulation seemed likely.

Boundary-layer wind maxima and jets can be explained by several mechanisms: (1) Inertial oscillation (Blackadar, 1957); (2) Thermal contrast produced by a sloped surface (McNider and Pielke, 1981); (3) Topographic effects produced by a flow forced above the barrier (DeSouza *et al.*, 1971; Hsu, 1979a); and, perhaps, (4) Transient pressure gradients associated with clouds. As Oliveira (1990) and Greco *et al.* (1992) have noted, none of these mechanisms is appropriate for understanding equatorial boundary-layer wind maxima. The inertial period at Manaus (3° S, site of the experiments) is about 5 days, and the first mechanism is ruled out. Topographic effects are confined to the extreme west and northern parts of the Amazon basin. The terrain elevation along the longitude at 60° W starting near Manaus rises gently 100 m above the MSL to approximately 200 m height at 4° N (Oliveira, 1990). At this longitude, the slope of the terrain is 1:2300 between 3° S and 4° N, where it abruptly increases from 300 to 600 m, well below the Great Plains terrain slope of 1:800 (Wexler, 1961). The horizontal pressure gradient estimated by assuming the buoyancy acceleration proportional to the vertical gradient of potential temperature times the elevation of the terrain is approximately two orders of magnitude lower than the horizontal pressure gradient observed at the surface (OF).

Another possible mechanism responsible for the observed afternoon evolution of boundary-layer winds and low-level wind maxima would be a circulation induced by preferential inland cloud formation. It is conceivable that the cloud-induced horizontal pressure gradients might also provoke jets similar in structure to those produced by a river breeze circulation. Scala *et al.* (1989) found that a mature Amazonian squall line can induce a horizontal pressure gradient equivalent to the amplitude of the diurnally-varying pressure gradient observed at the surface (OF). Similar order-of-magnitude estimates for the horizontal pressure gradient were obtained by Lemone *et al.* (1988). We cannot rule out this origin for the jet-like circulations, but we note that the jet wind direction would not be fixed geographically as was observed. A better answer awaits a more complete numerical simulation; we believe that cloud forcing is probably a consequence of river breeze triggering.

In this paper we examine the hypothesis that the presence of river breeze forcing associated with the wide rivers of the central Amazon region is a plausible explanation both for the nocturnal low level circulations and for the diurnal clockwise rotation of the surface wind vector that is observed (OF). The idea is that these diurnal patterns result from the cooperative effects of river breeze forcing and boundary-layer mixing. Our method is both analytic and numerical.

2. Linear Analysis of a River Breeze

Can a river 20 km wide induce a thermal circulation that is strong enough to affect the circulation 20 km away from the river? A mesoscale numerical simulation of a case of the Amazon river breeze by Miller *et al.* (1989) indicated formation of a very weak circulation, confined to the vicinity of the river. Observations presented by OF indicate that the observed river-induced circulation is much stronger. Theoretically, any thermal circulation induced by surface thermal contrast would extend vertically through the depth of the PBL (Pielke and Segal, 1986). If the vertical extent of the PBL were not predicted correctly, the strength of the river circulation would be underestimated. Another factor that may have contributed to the reduction of the river breeze in the mesoscale simulation could be the effect of the background circulation. During the day, the river breeze would be masked by the southerly component of the synoptic flow, and during the night the land breeze would be offset by this flow. Local winds observed near Manaus during ABLE 2a were particularly intense during the days used to initialize these simulations (on July 25 and August 03). On the other hand, the lack of a developed river breeze might also indicate that the river is not wide enough to support a thermal circulation as indicated by observation.

To assess the likelihood of the river breeze, we employed a simple linear sea breeze model (Rotunno, 1983), in which the horizontal extent of the thermal circulation is inversely proportional to the latitude, with the sea breeze penetrating deeper inland at lower latitudes. Linear inviscid results for latitudes less than 30° are unrealistic. In such circumstances, the model predicts that the circulation is 90° behind the forcing. Rotunno showed that including a linear friction term affects the sea breeze circulation by decreasing a phase lag between the heat forcing and the circulation. Dalu and Pielke (1989) modified Rotunno's model to simulate the low-latitude sea breeze. In this version, dissipative effects are introduced linearly. The inclusion of friction in the linear model leads to formation of a closed circulation, allowing solution in terms of a streamfunction. We use the Dalu and Pielke solution for diurnal cyclic forcing. To assess the plausibility of the river-breeze circulation, we ignore the transient aperiodic solutions. The dimensionless form of the streamfunction equation that describes the thermal circulation assuming thermal forcing periodic in time with frequency ω and steady state is:

$$\partial^2 \Psi'_R/\partial\zeta^2 + \partial^2 \Psi'_R/\partial\eta^2 = -\beta_2 \partial H'/\partial\zeta\,, \tag{1}$$

where Ψ'_R is the real part of the streamfunction, ζ and η are the dimensionless horizontal and vertical dimensions, β_2 is a constant and the thermal forcing $H' = H_0$ (see Table I). Following Rotunno (1983), thermal forcing associated with the river breeze is specified by the expression:

$$H' = (H'_0/\pi)\{\pi + \tan^{-1}[(x-d)/x_0] - \tan^{-1}[(x+d)/x_0]\exp(-z/z_0)\,, \tag{2}$$

TABLE I

Linear river breeze model parameters

Latitude	0°
Amplitude of thermal contrast	5 K
Forcing frequency (ω)	2π/day
Damping frequency (λ)	1.2ω
Static stability	3 K/km
Θ_0, reference potential temperature	300 K
$Z_0 = h$	500 m
River width ($2\,d$)	20 km
X_0	4 km

where $x - d$ and $x + d$ are the positions of the river banks for a river of width $2d$; x_0 and z_0 indicate the scale of the decay of the heat forcing; H_0, the amplitude of the thermal forcing, is made dimensionless using the characteristic scales T and H: $H_0' = H_0 T^3/H^{-1}$; $H_0 = g\omega\,\Delta T/\theta_0$, where g is gravitational acceleration, Θ_0 a reference potential temperature, ω is the frequency of the thermal forcing, and ΔT is the amplitude of the surface temperature contrast between the river and the forest. The form of the thermal forcing used in simulating the river breeze is similar to the form of the temperature cross-section observed over the Negro River (See Figure 6a in OF). According to (2), the spatial distribution of the thermal forcing is minimum negative over the river and maximum positive over the forest.

For convenience, the streamfunction equation was solved numerically using a simultaneous over-relaxation technique (Press *et al.*, 1986) on a 183 by 183 grid. Parameters (Table I) were chosen in accord with observations (OF), corresponding dimensionally to a vertical extent of 10 km and horizontal extent of 150 km. Boundary conditions specify no mass exchange through the boundaries. The time dependence of variables u, v, w, H, b and $\partial p/\partial x$ are indicated in Figure 1 for the parameters in Table I. Variables u and v are the cross- and along-river wind components, w the vertical wind speed, b is the buoyancy acceleration and $\partial\phi/\partial x$ is the cross-river horizontal pressure gradient. The u and w wind components are in phase with the streamfunction (Ψ), which in turn is in phase with the heat forcing (H). The cross-river horizontal pressure gradient and the along-river wind and buoyancy accelerations are 90° out of phase with the thermal forcing. The pressure gradient acceleration leads by an angle of atan(ϕ_p), where $\phi_p = (\omega/\lambda)(\lambda^2 + \omega^2 - f^2)/(\lambda^2 + \omega^2 + f^2)$ depends on the damping frequency λ, the Coriolis parameter f and the forcing frequency ω. The along-river wind speed and buoyancy lag the thermal forcing signal by an angle that depends on the assumed damping frequency λ. At the equator, the along-river wind speed is equal to zero and the buoyancy acceleration and the cross-river pressure gradient are respectively ahead and behind the heat forcing by approximately 40°. The phase shift

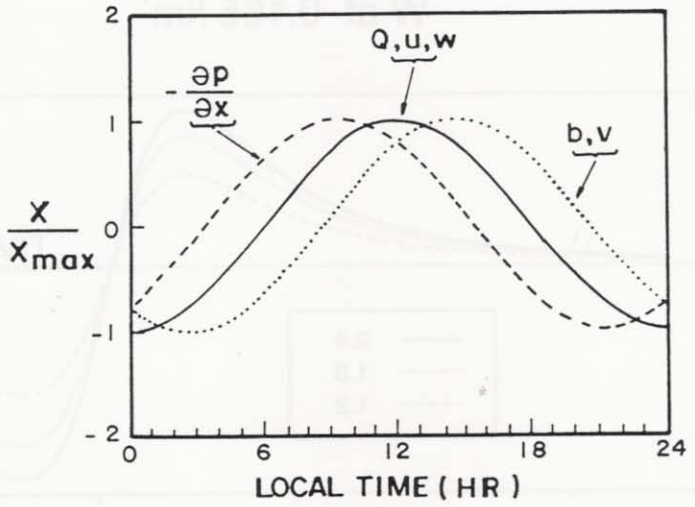

Fig. 1. Sketch of the temporal evolution of the linear river-breeze solution at the equator. Thermal forcing is assumed to vary harmonically at angular frequency ω with damping frequency λ equal to 1.2ω. The specific humidity (shown by Q), velocities u, and w (defined in text) are given by a solid line; buoyancy force b and along-river wind component v by a dotted line; and minus the perturbation pressure gradient $-\partial p/\partial x$ by a dashed line.

between the thermal forcing and the horizontal and vertical acceleration is small for a very rough surface such as the Amazon rain forest.

Figure 2 shows the results at the equator for a river 20 km wide, with damping frequency λ of 2.4ω, 1.8ω, and 1.2ω, the depth of the thermal forcing being 250 m, ΔT between the river and the forest 5 °C (corresponding to a 10 °C diurnal range of forest temperature), and other parameters as indicated in Table I. $\lambda = 1.2\omega$ corresponds most closely to the observed forcing. Extremes of vertical velocity are located near river edge, determined by the position of the maximum in the thermal forcing function. Modelled horizontal wind profiles are assymetrical on either side of the river, a feature found by the aircraft (OF, 1992, Figure 5a). Note the strong modelled subsidence over the river, as closed circulations at both sides of the river cooperate with each other.

Dimensionally, the horizontal pressure gradient at the surface is approximately 0.8–1.1 mb/100 km at the edges of the river, falling off to 0.20–0.25 mb/100 km at a distance of 20 km from the river bank. The order of magnitude of the horizontal pressure gradient near the river is comparable to that observed (see Figure 8, OF). Despite the level of simplification and the negative effect of the thermal dissipation on the intensity of the thermal forcing, the linear model gives a good idea of the order of magnitude of the dynamic parameters involved in the river breeze.

We conclude that the river breeze induced by the Negro river should affect the

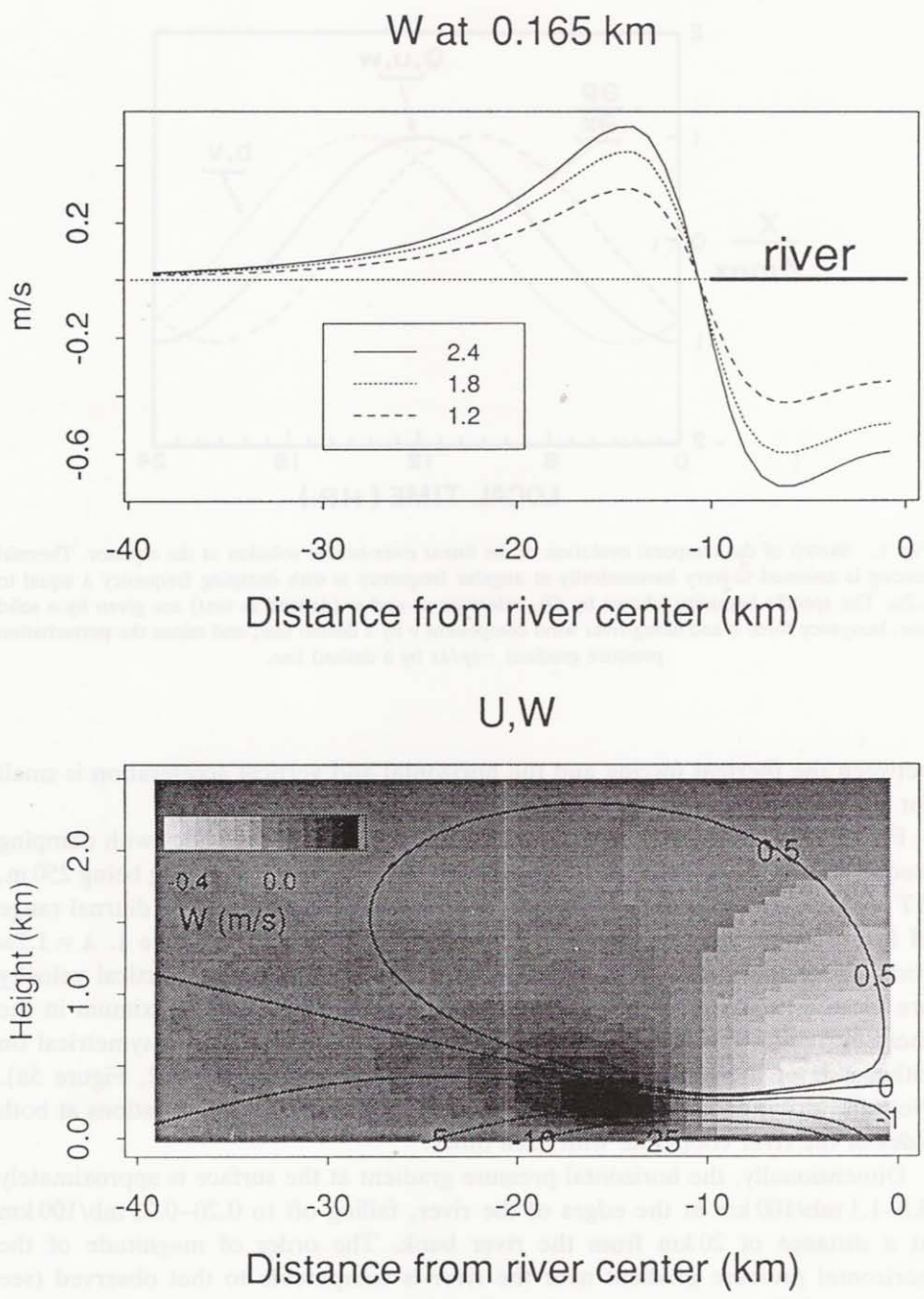

Fig. 2. Results of the linear solution for a 20 km wide equatorial river. Other parameters are given in Table I. Top: Vertical velocity at 0.165 km for three values of the damping frequency λ: 2.4ω (solid), 1.8ω (dotted), and 1.2ω (dashed). Bottom: Cross-section of the vertical velocity (shading) and horizontal velocity for the case $\lambda = 1.2\omega$. Velocities are in m/s.

surrounding regions significantly. Diurnal evolution of the low level circulation observed during the ABLE 2 experiments could plausibly have been produced by a horizontal pressure gradient induced by the river-forest thermal contrast. In a real boundary layer, surface friction would be expected to modify the horizontal wind pattern of Figure 2. At night, the wind maximum at the surface would be shifted upward and appear as a jet-like feature. In the day, vigorous convective mixing would tend to spread out the river breeze component through the entire convective boundary layer.

3.1. Mean equations, the equatorial basic state, and return to equilibrium

Surface winds depend on the relative importance of the convective momentum distribution of the basic state and perturbations caused by the river breeze. In this section we simulate the vertical evolution of the PBL over the Amazon rain forest for different amplitudes and vertical distributions of thermal forcing of a river breeze. We also study basic state wind fields characteristic of the wet and dry seasons, respectively. We concentrate on the formation of low level wind maxima, mechanisms of vertical redistribution of momentum in the PBL, and the impact of entrainment in the diurnal evolution of wind at the surface.

We model the river breeze as a perturbation from a basic state. In middle latitudes, the choice for the basic state is traditionally made by assuming that the free atmosphere is in geostrophic balance. Because the geostrophic balance is irrelevant in the equatorial tropics, the return-to-equilibrium condition results from an equilibrium defined by a balance between the horizontal pressure gradient force and horizontal advection. The modelled evolution of the potential temperature field will be constrained by an equilibrium between externally-imposed radiative cooling and the internally-simulated turbulent processes. The evolution of the mixing ratio field is described in a similar manner. These assumptions on the scalar balances were made by Sommeria (1976) to simulate the PBL in other tropical regions.

In the absence of a synoptic-scale disturbance and turbulent stress, the steady-state basic equations of motion at the equator are simply:

$$U_{j0}\partial U_{i0}/\partial x_j = -(1/\rho_0)\partial P_0/\partial x_i, \qquad i,j = 1,2\,, \tag{3}$$

where $U_{i0}(x, y)$ are the zonal and meridional components of the large-scale flow and P_0 is the large-scale pressure field.

The time-dependent perturbation from this mean state is:

$$\partial u_i/\partial t = -(1/\rho_0)\partial P/\partial x_i - \partial(\overline{u_i' w'})/\partial z + \{\partial U_i/\partial t\}_{\text{rest}}\,, \tag{4}$$

where $U_i(x, y, z, t) = U_{i0}(x, y) + u_i(z, t)$ are the components of the total wind in the disturbed region of the flow, $P(x, y, z, t) = P_0(x, y) + p(x, y, z, t)$ is the total pressure field and $(\overline{u_i' w'})$ is the Reynolds stress component. $\{\partial U_i/\partial t\}_{\text{rest}}$ is a "restoring acceleration" that relaxes the PBL back toward the base state, roughly in the

same way as does the geostrophic balance in midlatitudes. The time scale for the restoring process is related to the time scale of the inertial acceleration of the large-scale flow. The local rate of change of horizontal momentum associated with the effect of restoring to the basic state is:

$$\{\partial U_i/\partial t\}_{\text{rest}} = -(U_j - U_{j0})\partial U_{i0}/\partial x_j \approx -(U_i - U_{i0})/\tau\,; \tag{5}$$

here τ is characterized by the advective time scale of the large-scale flow, observed to be approximately one day.

If one assumes that the equatorial atmosphere is in approximate thermodynamic equilibrium on the time scale of a day, and neglecting horizontal advection of heat, the daily-averaged local rate of change of PBL temperature will be zero. In the free atmosphere, the average balance must be achieved between the vertical advection, radiative cooling and the condensation. In the case of the PBL, the balance also includes the vertical divergence of the turbulent flux.

Since $\partial\Theta/\partial z$ is small in the PBL, we neglect mean vertical advection, assuming that warming through entrainment during PBL growth and local cloud condensation is offset on a diurnal average by radiative cooling. The cooling rate induced by long-wave radiation, estimated using the Roach and Slingo (1979) radiation model, varied from -3.2 °C/d at the surface, to about -2.6 °C/d at 2000 m during the dry season (1985). During the wet season (1987), the atmosphere cooled less, approximately -2.6 °C/day throughout the 2000 m layer (G. G. Lala, personal communication, 1989). Based on these estimates, we imposed model radiative cooling that varies linearly in the vertical, from -1.5 °C/day at the surface to zero at 1500 m.

Similarly, if one assumes that the boundary-layer moisture content does not change in the scale of one day, and neglecting horizontal advection, the local change of mixing ratio integrated throughout the day and through the atmosphere should also be zero. In the free atmosphere, the balance is between the vertical advection and the condensation process, while in the PBL the balance is between the condensation process and divergence of vertical turbulent flux of moisture.

To simulate the process of removing moisture from the atmosphere by clouds, we assumed that the mixing ratio in the PBL is bounded by a fraction of the saturation mixing ratio, given by a maximum relative humidity of 90%. The amount of moisture removed is assumed to condense in cumulus clouds and precipitate locally. The qualitative results obtained are not greatly affected by the details of the relaxation conditions. Indeed, boundary-layer winds, temperatures, and humidity profiles were observed during ABLE-2 to relax toward a basic state on a 1–2 day time scale.

3.2. Second-order closure model (SOCM)

To simulate the mean flow within the PBL, we must estimate the Reynolds fluxes; this we did using a second-order closure technique. The SOCM consists of soiving the equations for the second-order moments of fluctuating quantities, obtained in

the Reynolds-averaged equations of motion and thermodynamics, by closing them tnrough parameterizations of the third-order moments (Donaldson, 1973). In their study using the Wangara experimental data, Yamada and Mellor (1975) presented one of the few PBL simulations using SOCM to reproduce the entire diurnal cycle. We adopt the parameterizations used by Mellor and Yamada (1982, MY82), as they have been calibrated with more recent data. Details of the model are given in Oliveira (1990). In addition to the prognostic equations for mean wind vector and scalar concentrations, the model consists of prognostic equations for the Reynolds stress components, the turbulent flux components, and the scalar variances:

Velocity variances ($i = 1, 2$, *no sum*):

$$\partial(\overline{u_i'u_i'})/\partial t = -2\overline{u_i'u_i'}\partial U_i/\partial z - [3\overline{u_i'u_i'} - e]/(3\tau_{IM}) - (2e/3\tau_{DM}) + \\ + \partial(K_M\partial\overline{u_i'u_i'}/\partial z)/\partial z$$

$$\partial(\overline{w'w'})/\partial t = 2(g/\Theta_0)\overline{w'\theta'} - [3\overline{w'w'} - e]/(3\tau_{IM}) - (2e/3\tau_{DM}) + \\ + \partial(K_M\partial\overline{w'w'}/\partial z)/\partial z$$

Stress covariances ($i = 1, 2$):

$$\partial(\overline{u_i'w'})/\partial t = (g/\Theta_0)\overline{w'u_i'} - \overline{w'w'}\partial U_i/\partial z - \overline{u_i'w_i}/\tau_{IM} + \\ + \partial(K_M\partial\overline{u_i'w'}/\partial z)/\partial z$$

Flux covariances ($x = \theta, q$):

$$\partial(\overline{u_i'x'})/\partial t = -\overline{u_i'x'}\partial U_i/\partial z - \overline{u_i'w'}\partial X/\partial z - [\overline{u_i'x'}]/\tau_{Ix} + \\ + \partial(K_x\partial\overline{u_i'x'}/\partial z)/\partial z$$

Scalar variances ($x = \theta, q$):

$$\partial(\overline{x'x'})/\partial t = -2\overline{w'x'}\partial X/\partial z - [\overline{x'x'}]/\tau_{Dx} + \partial(K_x\partial\overline{x'^2}/\partial z)/\partial z\,,$$

where $e = \overline{u_i'u_i'}$ is twice the turbulent kinetic energy. The τ_D are the characteristic time scales of molecular dissipation of momentum (M), scalar variance for θ and q (x); τ_I are the characteristic time scales for destruction of covariance of momentum (M), scalars θ and $q(x)$, and redistribution of variance of momentum (M) induced by the tendency-to-isotropy term; K is a coefficient of turbulent diffusion of variance and covariance of these variables, parameterized as $K_M = 0.12\,l\,e^{0.5}$; $K_x = 0.2\,l\,e^{0.5}$. The characteristic time scales are parameterized as: $\tau_{DM} = 16.6\,l\,e^{-0.5}$, $\tau_{Dx} = 10.1\,l\,e^{-0.5}$, $\tau_{IM} = 0.92\,l\,e^{-0.5}$, where l is the master length scale. While MY82 assumed l to be proportional to the height above the ground at low levels and constant above, we set the master length scale equal to: $1/l = 1/\kappa z + 1/l_0 + 1/(z_T - z + \epsilon)$, where κ is the von Karman constant, z_T is the top of the model, $\epsilon = 0.1$, and $1/l_0 = 10\int e^{0.5}\,dz/[\int z\,e^{0.5}\,dz]$, where the integration is from the surface layer to the top of the model.

We introduced the last term including ϵ in the definition of the master length scale to avoid spurious oscillations in the variance fields. A solution of a model that simulates turbulent flow is said to be realizable when it satisfies the existence conditions pointed out by Schumann (1977) for Reynolds stress. Our conditions guarantee non-negative turbulent kinetic energy and a correlation coefficient not larger than one. In this version on the SOCM, realizability is assured by the clipping condition (André *et al.*, 1975). Further details are presented in Oliveira (1990).

3.3. Numerical considerations

The finite difference scheme used is forward in time and centered in space, with a vertically staggered linear grid with 81 levels using an equally spaced grid of 12.5 m to a total height of 2000 m. A linear grid was chosen instead of the logarithmic grid commonly used in SOCM to provide better resolution in middle layers for simulations of the low level wind maxima. The upper boundary condition for the mean equations is zero vertical turbulent flux divergence at 20 m above the surface. The PBL rarely grows above 1500 m in the Amazon rain forest (Martin *et al.*, 1988).

Bottom boundary conditions are set up consistent with the equations describing the mean and the variance and covariance of momentum, temperature and mixing ratio at the level of surface, assumed to be the height of the roughness length. In the case of the mean quantities, the surface temperature and mixing ratio are evaluated by the heat budget at the surface. In the case of the turbulence quantities, we used the expressions derived by Mellor and Yamada (1974). These expressions are all evaluated in terms of u_*, θ_* and q_*, which in turn are determined by the surface heat balance.

3.4. Surface heat budget

Brost and Wyngaard (1978) simulated the nocturnal evolution of the stable layer with a simplified version of the second-order closure model. They found that the height of the stable PBL converges to a steady state when the cooling rate of the surface is specified. When they included the heat budget at the surface to diagnose the cooling rate of the surface, the stable PBL never reached steady state. These results suggested that the nocturnal evolution of the PBL is highly dependent on the initial state and the surface fluxes (also noted by Nieuwstadt and Tennekes, 1981). To evaluate the lower boundary conditions, the temperature, mixing ratio and the turbulent vertical fluxes of momentum, sensible and latent heat are determined by the heat budget equation so that the sensitivity to changes in the surface characteristics (roughness, emissivity, Bowen ratio) in the diurnal evolution of the PBL can be evaluated. Modeling the surface heat budget draws empirically on the ABLE 2 data when necessary. The surface heat balance is:

$$Q_h + Q_e - (I_s + I_r + I_a + I_g) + S_a + S_g - G = 0\,,$$

TABLE II
PBL simulation parameters

Latitude	0°
Solar declination	0°
Bowen ratio	0.3
Effective surface emissivity (ϵ)	1.9
Roughness parameter	1 m
Model height	2 km
Number of grid points	81
Time step	2.5 s

where Q_h is the sensible heat flux, Q_e is the latent heat flux; I_s is the incoming solar radiation; I_r the fraction of incoming solar radiation reflected by the surface; I_a is the incoming long-wave radiation from the atmosphere; I_g is the outgoing long-wave radiation from the surface; G is the soil heat flux at the surface; S_{ac} and S_g are the amounts of heat stored by the system atmosphere-forest and by the soil, respectively. Vertical fluxes are defined positive upwards.

The incoming solar radiation is given by $I_s = -I_0 \cdot \mathrm{Tr}\cos(z)$ (Stull, 1988, Ch. 7), where I_0 is the solar constant (1380 W/m^2), z is the zenith angle and Tr is the atmospheric transmissivity. The transmissivity (Tr) used in the model is based on approximately 30 days of hourly averaged values of incoming solar radiation measured during ABLE 2b: $\mathrm{Tr} = 0.22 + 0.18\cos(z)$, $a = 0.31 - 0.20\cos(z)$. No published expression is available to evaluate the atmospheric lonng-wave radiation over the Amazon region in terms of surface parameters (temperature, moisture, cloud cover). The incoming long-wave radiation was evaluated according to Kondo and Gambo (1979): $I_a = -(0.52 + 0.064r\ e^{0.5})\sigma T_a^4$, where e is the mean vapor pressure (set equal to 20 mb), T_a is the mean atmospheric temperature near the surface and σ is the Stefan-Boltzmann constant. T_a is assumed to be equal to the temperature at the second level of the model.

The outgoing long-wave irradiance from the surface was evaluated by considering the surface to be radiating as a gray body at the equivalent blackbody temperature (T_e). The Stefan-Boltzman law can be applied according to the expression: $I_g = \epsilon\sigma T_e^4$ where ϵ is the emissivity of the surface, T_e is the equivalent blackbody temperature. Since there is no simple way to evaluate the equivalent blackbody surface temperature, we assumed that the top of the canopy is an equivalent rigid surface and considered the difference between the actual temperature at the surface and the equivalent blackbody temperature of the "surface" by modifying the emissivity for the whole surface, as indicated by the parameter given in Table II. The emissivity of the real surface is assumed to be 1.0 (Sellers, 1988).

For simplicity, the bulk transfer method was used to evaluate the surface turbulent fluxes: $u_*\theta_* = -C_h\langle U\rangle(\langle T\rangle - T_s)$, where u_* and θ_* are respectively the characteristic scales of velocity and temperature of the surface layer; $\langle U\rangle$ and $\langle T\rangle$ are averaged values (through the surface layer) of horizontal wind speed and

temperature; T_s is the surface temperature and C_h is the sensible heat turbulent flux transfer coefficient. Moisture flux is parameterized in the same manner. Heat transfer coefficients are those of Deardorff (1968). The drag coefficient at 5 m above the forest canopy varies from 0.010 during the nighttime to 0.100 during the day (Fitzjarrald *et al.*, 1988). The neutral drag coefficient is found using a logarithmic wind profile assuming the roughness length to be 1 m (Stull, 1988) and the displacement length of the Amazon Forest to be 0.75 of the approximate height of the canopy (40 m, Shuttleworth *et al.*, 1984).

Because the observations indicated that the bulk of the heat moisture flux occurs during the daytime, for simplicity we used a constant Bowen ratio equal to the observed daytime value of 0.30 (Abreu Sá *et al.*, 1986). Heat stored in the canopy-atmosphere system was assumed to be (Moore and Fisch, 1986):

$$S_{ac} = \{S_T + S_q[L/R_v]q_s(T_s)/T_s\}\,\mathrm{d}T/\mathrm{d}t, s\,,$$

where S_T and S_q are respectively equal to 23.86 J/K·m^2 and 40.0 J·g/kg·m^2, $\mathrm{d}T/\mathrm{d}t$ the rate of change of temperature observed at the top of the canopy, L is the latent heat of evaporation, R_v is the gas constant for the water vapor, $q_s(T_s)$ is the saturation mixing ratio at the temperature of the surface, T_s is the surface temperature. Our canopy heat storage expression was derived from the Moore and Fisch relation assuming that the air within the canopy is close to saturation.

3.5. Free Convection

To allow for the common situation of approximately free convection, the temperature of the surface was evaluated differently when the bulk Richardson number is above the one considered critical. The expression used to evaluate the sensible heat flux at the surface is given by: $u_*\theta_* = -C_{hF}(\langle T\rangle - T_s)$, where C_{hF} is given by (Zhang and Anthes, 1982):

$$C_{hF} = \{C_h(\mathrm{Ri}_*)^2_B g\delta z(\langle T\rangle - T_s)^{0.5}\}[\Theta_0(\mathrm{Ri}^*)_B]^{-1}$$

where $C_h(\mathrm{Ri}^*)_B$ is the heat transfer coefficient obtained from the Deardorff (1968) expression for the critical bulk Richardson number, g is gravitational acceleration, δz is the thickness of the surface layer and Θ_0 is the reference temperature set equal 295 K. The limit between forced convection and free convection is not precisely established in the literature. In the model, we have assumed a critical Richardson number equal to -0.5, corresponding to $z/L \approx -5$, where L is the Obukhov length. Free convection is observed to occur when $z/L < -1$ (Panofsky and Dutton, 1984, p. 185).

4. Boundary-Layer Model Results

The linear model presented in Section 2 indicated that a river 20–40 km wide is able to support a river breeze with a thermal amplitude of the order of 5 °C that extends vertically through the first 500 m. The amplitude of the horizontal pressure

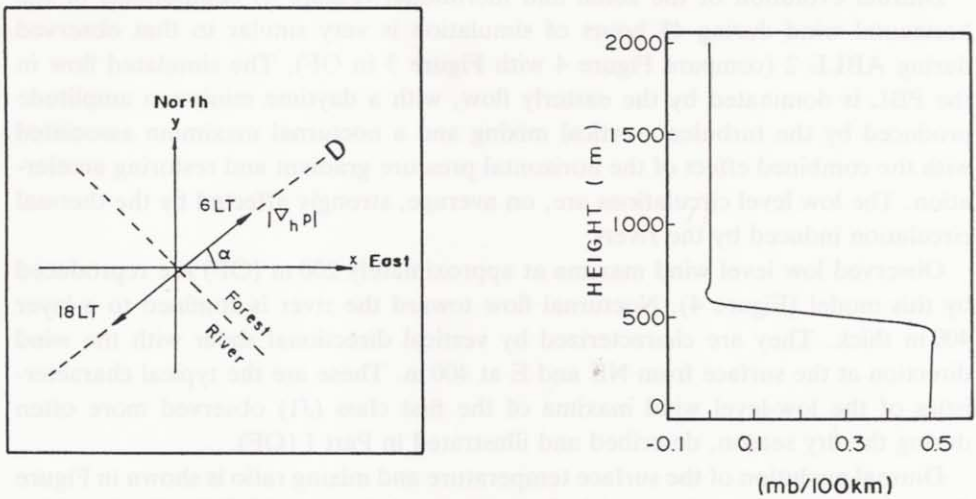

Fig. 3. Left: Coordinate system for simulation; Right: Vertical distribution of the horizontal pressure gradient.

gradient induced in the linear model is of the order of 0.2–0.25 mb/100 km around 10–20 km away from the river. The objective of simulations is to understand the diurnal evolution the PBL in the region. To accommodate the main characteristics of the equatorial PBL, numerical simulations were designed by assuming that the basic state is such that the horizontal wind is a 10 m/s easterly flow. Initially, the vertical profile of horizontal wind is set equal to the basic state, and the vertical profile of potential temperature and mixing ratio are set equal to the average values observed during the ABLE 2a dry season experiment (OF).

The magnitude of the horizontal pressure gradient as well as its time evolution are prescribed based on the surface data analysis. The horizontal pressure gradient is oriented in the direction D that forms an angle α with the X-direction (Figure 3, left panel). Its vertical distribution (Figure 3, right panel) is hypothesized in terms of the idealized thermal circulation from the river breeze linear model simulations in the Section 2. The horizontal pressure gradient is assumed to be 180° in the negative D direction during the daytime hours, and in the D direction at night. The maximum amplitude of the horizontal pressure gradient is set at 18 LT (out of phase) and 6 LT (in phase). This timing is equivalent to positioning the river to the southwest and the forest to the northeast. The time scale of the restoring terms in the horizontal momentum equation, evaluated by dividing the length scale of the large-scale pressure gradient (1000 km) by the characteristic wind speed, is approximately 28 hours. The externally imposed parameters used in the numerical simulation of the PBL are indicated in Table II. A solar declination equal to zero was chosen for simplicity.

Diurnal evolution of the zonal and meridional (Figure 4) components of the horizontal wind during 48 hours of simulation is very similar to that observed during ABLE 2 (compare Figure 4 with Figure 3 in OF). The simulated flow in the PBL is dominated by the easterly flow, with a daytime minimum amplitude produced by the turbulent vertical mixing and a nocturnal maximum associated with the combined effect of the horizontal pressure gradient and restoring acceleration. The low level circulations are, on average, strongly affected by the thermal circulation induced by the rivers.

Observed low level wind maxima at approximately 200 m (OF) are reproduced by this model (Figure 4). Nocturnal flow toward the river is confined to a layer 400 m thick. They are characterized by vertical directional shear with the wind direction at the surface from NE and E at 400 m. These are the typical characteristics of the low-level wind maxima of the first class (*J*1) observed more often during the dry season, described and illustrated in Part I (OF).

Diurnal evolution of the surface temperature and mixing ratio is shown in Figure 5. Amplitudes are consistent with those observed during ABLE 2b (Fitzjarrald *et al.*, 1988). Radiational and turbulent components of the surface heat budget evaluated as a boundary condition are shown in Figure 5. The magnitude of the simulated turbulent heat and momentum fluxes and the surface temperature are comparable to observations (Shuttleworth *et al.*, 1984, Fitzjarrald *et al.*, 1988, 1990). Modelled forest canopy heat storage has the amplitude and phase observed by Moore and Fisch (1986).

During the daytime, considerable divergence of mòmentum flux is responsible for the large variations in the zonal and meridional momentum (Figure 6). With the onset of surface-layer stability at night, the vertical turbulent flux of momentum decreases considerably and variations in mean flow are controlled mainly by the hypothesized restoring acceleration (in the zonal direction only) and by the horizontal pressure gradient. Vertical profiles of mean potential temperature and mixing and their vertical turbulent fluxes are shown in Figure 7. During the daytime, the sensible and latent heat fluxes vary linearly with height within the PBL, consistent with the expected approximate mixed-layer structure for the potential temperature and mixing ratio. Simulated growth and structure of the convective boundary layer closely resemble observations presented by Martin *et al.* (1988). At night, turbulence is low below 200 m. Variations in the mean quantities above the surface layer are largely controlled by the nonturbulent processes.

Another observed feature simulated by the model is the elliptical shape of the diurnal cycle, apparent in the polar plot of surface-wind perturbation from the diurnal mean (Figure 8). The clockwise rotation rate of the perturbation surface wind vector is close to that observed. The mean wind vector rotates approximately 90° ahead of the horizontal pressure gradient. Orientation of the mean flow with the horizontal pressure has a strong impact on the orientation of the ellipses traced by the perturbation surface wind vector through the day. The ellipses in Figure 8

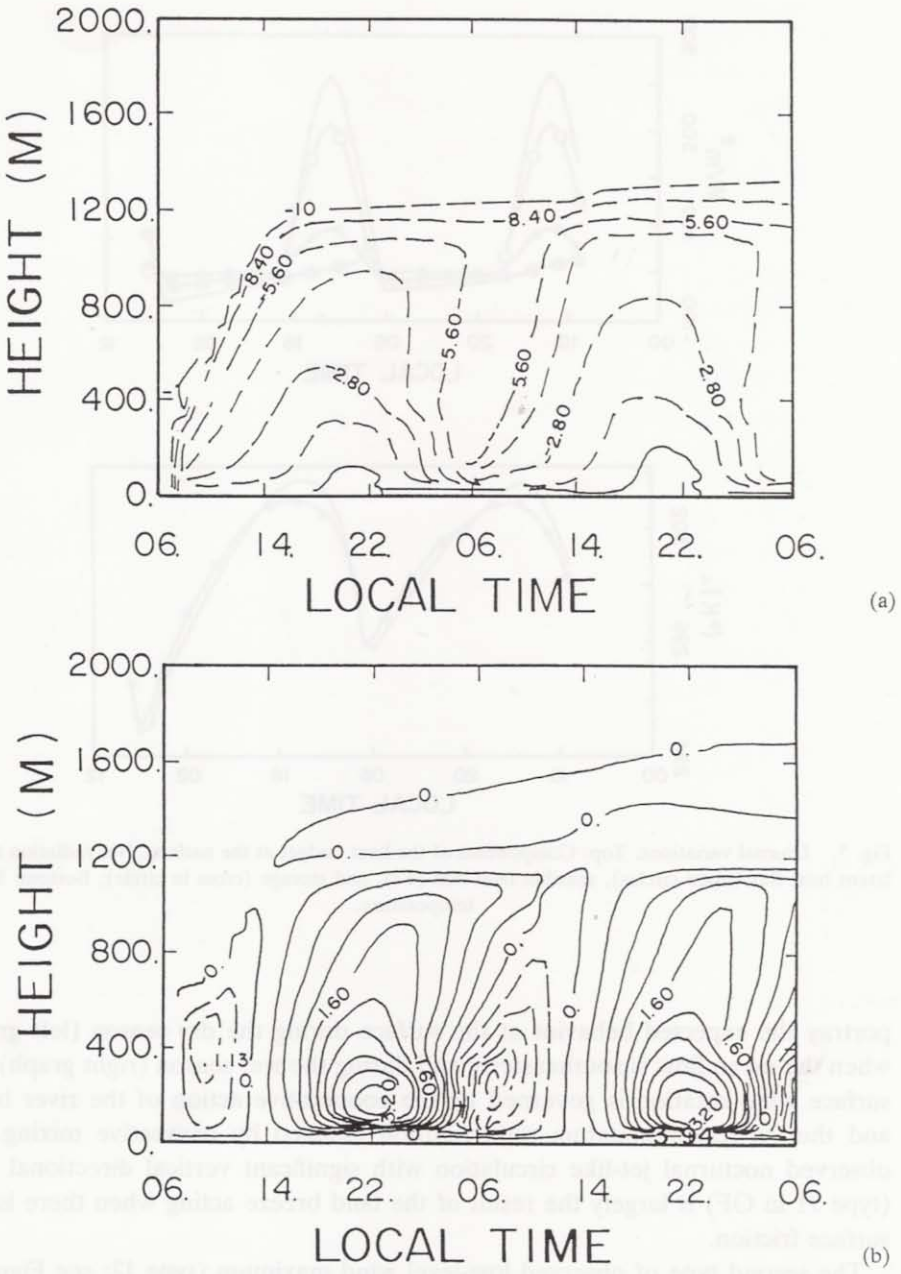

Fig. 4. Simulated diurnal evolution of: (a) Zonal component of the wind (m/s); (b) Meridional component of the wind (m/s). The abscissa corresponds to local time.

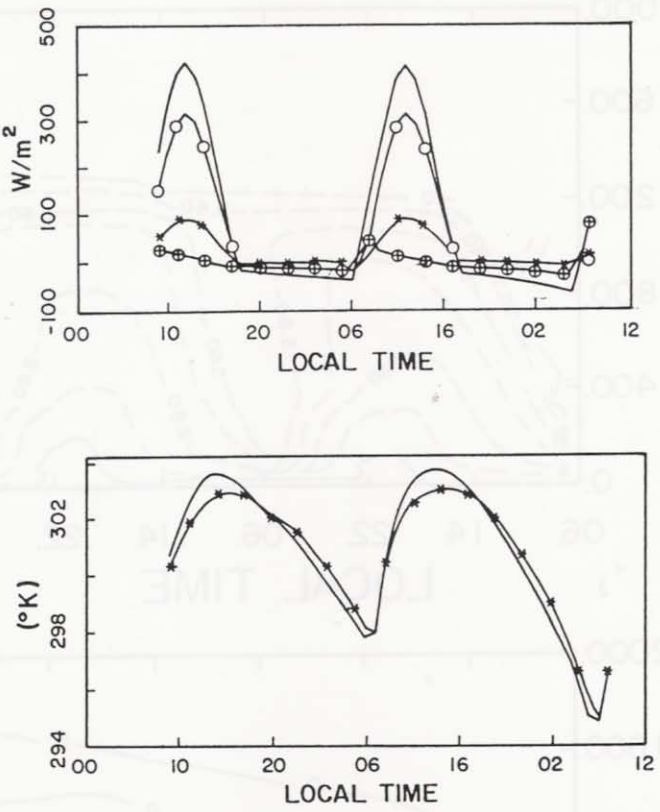

Fig. 5. Diurnal variations. Top: Components of the heat budget at the surface. Net radiation (solid), latent heat flux (open circles), sensible heat flux (x's), and storage (cross in circle); Bottom: Surface temperature.

portray the expected behavior at the surface during the dry season (left graph), when the mean flow is southeasterly and during the wet season (right graph). The surface wind rotation is governed by the cooperative action of the river breeze and the vertical momentum redistribution induced by convective mixing. The observed nocturnal jet-like circulation with significant vertical directional shear (type *J*1 in OF) is largely the result of the land breeze acting when there is little surface friction.

The second type of observed low-level wind maximum (type J2; see Figure 12 in OF) showed little directional wind shear. A sensitivity test increasing the intensity of the background wind indicated a possible mechanism for the formation of this type of wind maximum. Figure 9 illustrates the vertical profile of the zonal wind simulated from an initial baroclinic initial condition in which the zonal wind at the surface is equal to -20 m/s, decreasing linearly to -10 m/s at 1500 m. Under these circumstances a low-level wind maximum developed at the top of the

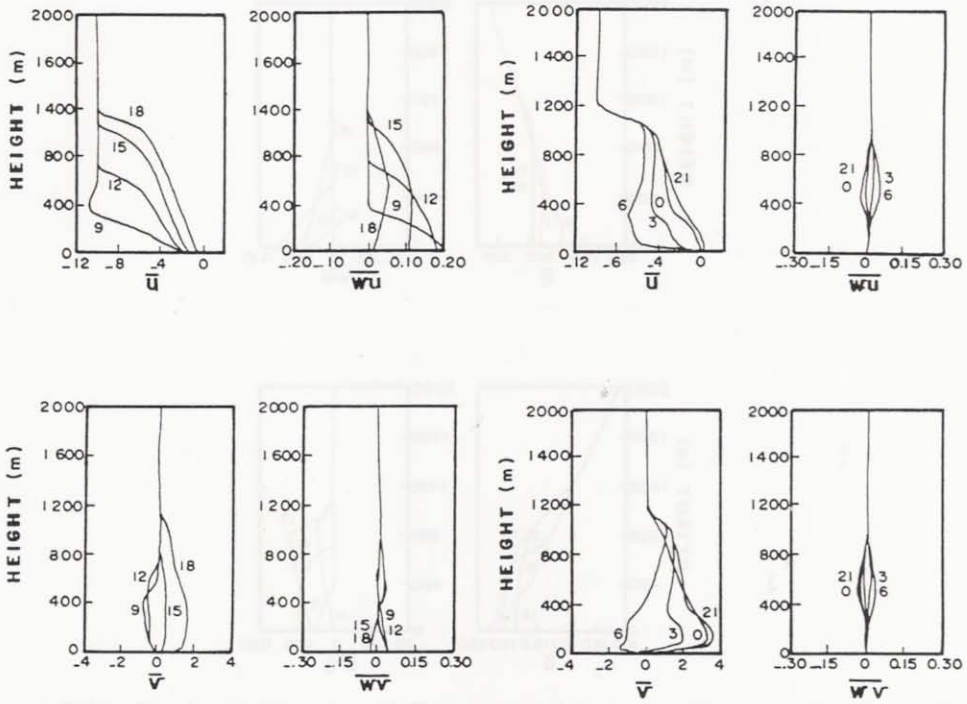

Fig. 6. Components of the mean wind (U and V, m/s) and Reynolds stress $\overline{w'u'}$ and $\overline{w'v'}$ (m^2/s^2). Local times are indicated.

PBL, and propagated upward. We hypothesize that the low-level wind maximum of the second class (J2, OF) may be induced by such a large-scale horizontal pressure gradient, but confirmation awaits more complete observations.

One of the consequences of widespread deforestation along the river banks in the Amazon would be to change the surface heat balance, perhaps reducing evapotranspiration. We looked at the consequences of setting the Bowen ratio at the surface to 10, holding other variables constant. The enhanced surface heat flux led to a deeper daytime mixed layer. In addition, the nocturnal stable layer became more intense, and there was a stronger jet-like wind profile induced by the land breeze. In a more realistic simulation, one would have to allow for enhanced river breeze pressure gradient forcing as well. This would perhaps be better addressed using a more complex model than that used here.

5. Conclusions

Many features of the dynamics of the PBL in the region of the experiment are uniquely determined by the combined effect of the river breeze induced by the

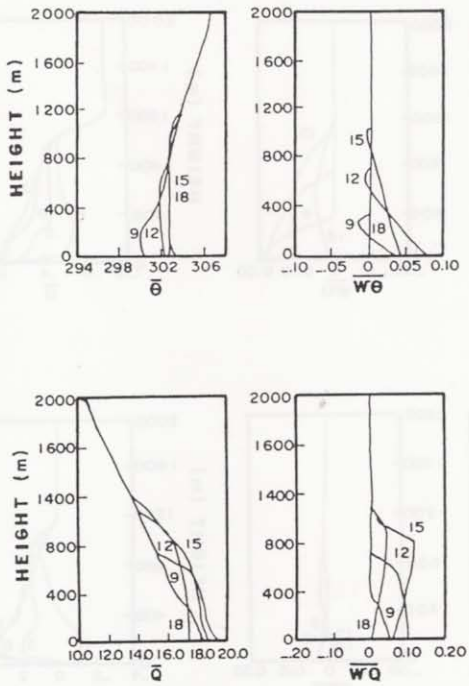

Fig. 7. Top: Vertical profiles of potential temperature (Θ, K) and sensible heat flux (K m/s); Bottom: Mixing ratio (g/kg) and latent heat flux (g/kg s). Model results for the first 24 hours at 9, 12, 15 and 18 LT.

Negro and Amazonas rivers, the easterly large-scale flow, and turbulence generated at the surface:

(1) The similarity between the cross-river circulation and temperature at the surface simulated by the linear model and that observed by the aircraft is strong evidence of the presence of river breezes near the great rivers of Amazonia;

(2) Sensitivity tests using the linear model indicated that an adequate choice of static stability, friction and depth of heating leads to an intensification of the simulated thermal circulation. In the simulations most similar to the observations, the horizontal pressure gradient is of the order of the 0.25 mb/100 km 20 km far from the river;

(3) Simulations of the PBL using a second-order closure model (SOCM) subject to a time-varying pressure gradient similar to river-breeze forcing successfully reproduce the observed diurnal changes in boundary-layer structure;

(4) Second-order closure model results indicated that the approximately elliptical shape and the sense of rotation of the observed surface wind is a result of the combined effects of the vertical redistribution of momentum associated with the diurnal evolution of the PBL and the thermal circulation embedded in a shear environment;

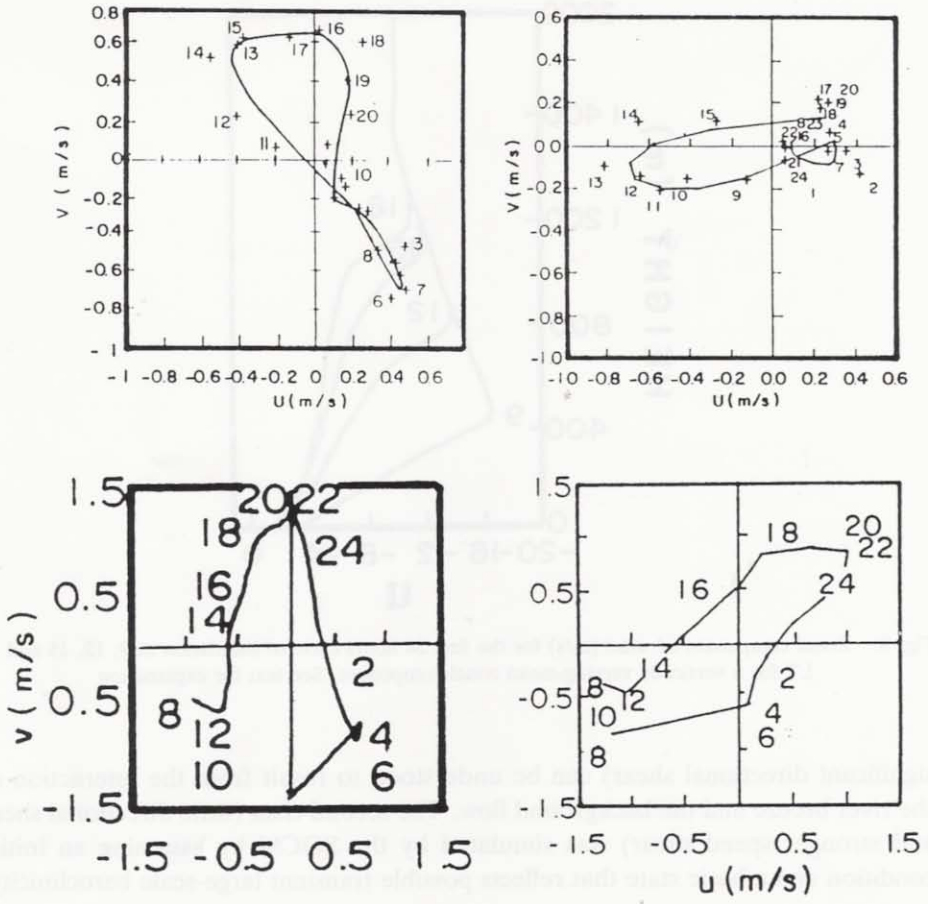

Fig. 8. Observed (top) and simulated (bottom) polar plots of the wind deviation from the diurnally average at the surface. The top two panels are hourly-averaged surface wind deviation from the diurnal mean at Ducke Reserve. Left: Ducke Reserve during the entire dry season experiment 1985 (July 15–August 5, 1985). Right: PAM II data obtained during the second period of the wet season experiment (April 28–May 13, 1987). Numbers correspond to Local Time. Points are the actual values and the continuous lines are the smooth curve through these points. The bottom two panels are results of simulation during the first 24 hours of simulation for the dry season (left) and wet season (right) basic flow simulations. Hours (LT) are shown.

(5) The SOCM sensitivity tests indicated that the evolution of the equatorial PBL is relatively insensitive to modest changes in Bowen ratio and roughness length. On the other hand, the sensitivity tests indicate that a change in the direction of the horizontal pressure gradient with respect to the background wind field resulted in the change in the orientation of the polar plot of the wind at the surface. This different orientation is the most significant seasonal difference in the region;

(6) The first class of low-level wind maxima identified in the observations (OF,

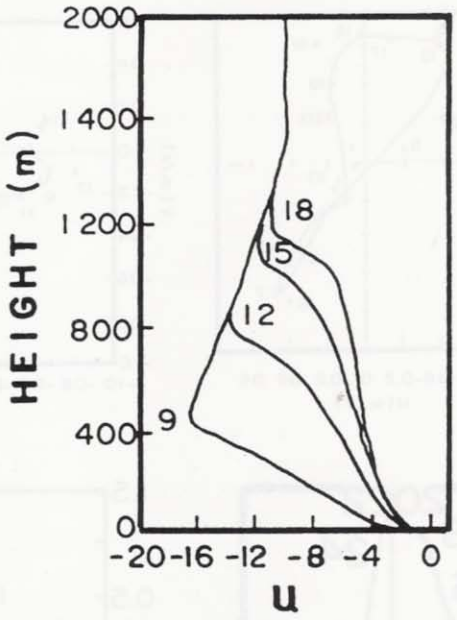

Fig. 9. Zonal component of wind (m/s) for the first 24 hours cycle of simulation at 9, 12, 15 and 18 LT for a vertically varying mean zonal component. See text for explanation

significant directional shear) can be understood to result from the interaction of the river breeze and the background flow. The second class (little directional shear and stronger speed shear) was simulated by the SOCM by assuming an initial condition and a basic state that reflects possible transient large-scale baroclinicity.

Acknowledgements

We are grateful to the Brazilian and American members of the ABLE-2 field team. Between 1985 and 1988, this work was supported by NASA grants NAG-1-692 and NAG-1-583 to the Atmospheric Sciences Research Center (ASRC), SUNY Albany. Continuing efforts have been supported by ASRC and by the Dept. de Ciencias Atmosféricas, U. of São Paulo. A. P. Oliveira acknowledges support of the Fundacão de Amparo a Pesquisa de São Paulo, Proc. 86/1263–6 during graduate studies at SUNY Albany.

References

Abreu Sá, L. D., Viswanadham, Y., and Manzi, A. O.: 1986, *Energy Receipt Partitioning over the Amazon Forest. Relatorio Tecnico*, INPE-3980–PRE/990, Instituto de Pesquisas Espaciais, São José dos Carnpos, SP, Brazil.

André, J. C., De Moor, G., Lacarrere, P., and du Vachat, R.: 1975, 'Turbulence Approximation for Inhomogeneous Flows: Part I. The Clipping Approximation', *J. Atm. Sci.* **33**, 476–481.

Blackadar, A. K.: 1957, 'Boundary Layer Wind Maxima and their Significance for the Growth of Nocturnal Inversions', *Bull. Am. Meteorol. Soc.* **38**, 283–290.

Brost, R. A. and Wyngaard, J. C.: 1978, 'A Model of the Stably Stratified Planetary Boundary Layer', *J. Atm. Sci.* **35**, 1427–1440.

Burk, S. D.: 1977, 'The Moist Boundary Layer with a Higher Order Turbulence Closure Model', *J. Atm. Sci.* **34**, 629–638.

Dalu, G. A. and Pielke, R. A.: 1989, 'An Analytical Study of the Sea Breeze', *J. Atm. Sci.* **46**, 1815–1825.

DeSouza, R.L., Aspliden, C. I., Garstang, M., Leseur, N. E., and Hsu, Y.: 1971, 'A Low Level Jet in the Tropics', *Mon. Wea. Rev.* **99**, 559–564.

Deardorff, J.: 1968, 'Dependence of Air-Sea Transfer Coefficients on Bulk Stability', *J. Geophys. Res.* **73**, 2549–2557.

Donaldson, C. DuP.: 1973, 'Construction of a Dynamic Model of the Production of Atmospheric Turbulence and Dispersal of Pollutants', in D. A. Haugen (ed.), *Workshop on Micrometeorology*. Am. Meteorol. Boston, 392 pp.

Fitzjarrald, D., Stormwind, B., Fisch, G., and Cabral, O.: 1988, 'Turbulent Transport Observed Just Above the Amazon Forest', *J. Geophys. Res.* **93**(D2), 1551–1563.

Fitzjarrald, D., Moore, K., Scolar, J., Cabral, O., Manzi, A. O., and Sá, L. D.: 1990, 'Daytime Turbulent Exchange Between the Amazon Forest and the Atmosphere', *J. Geophys. Res.* **95**(D10), 16825–16838.

Greco, S., Ulanski, S., Garstang, M., and Houston, S.: 1992, 'Low-Level Nocturnal Maximum over the Central Amazon Basin', *Boundary-Layer Meteorol.* **58**, 91–115.

Harriss, R. C., Garstang, M., Wofsy, S. C., Browell, E. V., Molion, L. C. B., MacNeal, R. J., Hoell, J. M., Bendura, R. J., Beck, S. M., Navarro, R. L., Riley, J. T., and Snell, R. L.: 1988, 'The Amazon Boundary Layer Experiment (ABLE 2A): Dry Season 1985', *J. Geophys. Res.* **93**, 1351–1360.

Harriss, R. C., Wofsy, S. C., Garstang, M., Beck, S. M., Bendura, R. J., Coelho, J. R. B., Drewry, J. W., Hoell, J. M., Matson, P. A., MacNeal, R. J., Molion, L. C. B., Navarro, R. L., Rabine, V., and Snell, R. L.: 1990, 'The Amazon Boundary Layer Experiment: Wet Season 1987', *J. Geophys. Res.* **95**, 16721–16736.

Kondo, H. and Gambo, K.: 1979, 'The Effect of the Mixing Layer on the Sea Breeze Circulation and the Diffusion of Pollutants Associated with Land-Sea Breezes', *J. Meteorol. Soc. Japan* **57**, 560–575.

Hsu, S. A.: 1979, 'Mesoscale Nocturnal Jet-Like Winds Within the Planetary Boundary Layer over a Flat, Open Coast', *Boundary-Layer Meteorol.* **17**, 485–495.

Lemone, M. A., Barnes, G. M., Fankhauser, J. C., and Tarleton, L. F.: 1988, 'Perturbation Pressure Fields Measured by Aircraft around the Cloud-Base Updraft of Deep Convective Clouds', *Mon. Wea. Rev.* **116**(2), 313–327.

Martin, L. C., Fitzjarrald, D., Garstang, M., Oliveira, A. P., Greco, S., and Browell, E.: 1988, 'Structure and Growth of the Mixing Layer over the Amazonian Rain Forest', *J. Geoph. Res.* **93**, 1361–1375.

McNider, R. T. and Pielke, R. A.: 1981, 'Diurnal Boundary-Layer Development over Sloping Terrain', *J. Atm. Sci.* **38**, 2198–2212.

Mellor, G. L. and Yamada, T.: 1974, 'A Hierarchy of Turbulence Closure Models for Planetary Boundary Layers', *J. Atm. Sci.* **31**, 1791–1482.

Mellor, G. L. and Yamada, T.: 1982, 'Development of a Turbulence Closure Model for Geophysical Fluids Problems, Reviews of Geophysics and Space Physics', **20**, 851–875.

Miller, W. F., Pielke, R. A., Garstang, M., and Greco, S.: 1989, 'Simulations of the Mesoscale Circulation in the ABLE II Region', *Proc. Third Intern. Conf. on Southern Hermisphere Meteorology and Oceanography*, Nov. 13–17, Buenos Aires.

Moore, C. J. and Fisch, G.: 1986, 'Estimating Heat Storage in Amazonian tropical Forest', *Agricult. Forest Metorol.* **38**, 147–169.

Nieuwstadt, F. T. and Tennekes, H.: 1981, 'A Rate Equation for Nocturnal Boundary Layer Height', *J. Atm. Sci.* **38**, 1418–1428.

Oliveira, A. P.: 1990, 'The Dynamics of the Planetary Boundary Layer over the Amazon Rain Forest,

Ph. D. dissertation, Department of Atmospheric Sciences, State University of New York, Albany, 296 pp.

Oliveira. A. P. and Fitzjarrald, D. R.: 1992, 'The Amazon River Breeze and the Local Boundary Layer: I, Observations', *Boundary Layer Meteorol.* **63**, 141–162.

Pielke, R. A. and Segal, M.: 1986, 'Mesoscale Circulations Forced by Differential Terrain Heating', 516–548. Chapter 22 of *Mesoscale Meteorology and Forecasting*, Edited by P. S. Ray, p. 793.

Press, W. H., Flannery, B. P., Teukolsky, S. A., Vetterling, W. T.: 1986, *Numerical Recipes: The Art of Scientific Computing*, Cambridge University Press, Cambridge, p. 818.

Roach, W. T. and Slingo, A.: 1979, 'A High Resolution Infrared Radiative Transfer Scheme to Study the Interactions of Radiation with Cloud', *Quart. J. R. Meteorol. Soc.* **105**, 603–614.

Rotunno, R.: 1983, 'On the Tinear Theory of the Land and Sea Breeze', *J. Atm. Sci.* **40**, 1999–2000.

Schumann, U.: 1977, 'Realizability of Reynolds-Stress Turbulence Models', *Physics Fluids* **20**, 721–725.

Sellers, P. J.: 1988, 'Modelling Effects of Vegetation on Climate: *The Geophysiology of Amazonia Vegetation and Climate Interactions*, Ch. 16, 297–344, R. E. Dickinson (ed.), John Wiley Sons, 526 pp.

Shuttleworth, W. J., Gash, J., Lloyd, J., Moore, C. J., Robert, C. J., Filho, A., Fisch, G., Filho, V., Ribeiro, M., Molion, L., de Abreu Sá, L., Nobre, C., Cabral, O. M. R., Patel, S. R., and Moraes, J. C.: 1984; 'Observations of Radiation Exchange Above and Below Amazonian Forest', *Quart. J. Roy. Meteorol. Soc.* **110**, 1163–1169.

Sommeria, G.: 1976, 'Three-Dimensional Simulation of Turbulent Processes in an Undisturbed Trade Wind Boundary Layer', *J. Atm. Sci.* **33**, 216–241.

Stormwind, B. L.: 1988, 'Turbulent Transport Above the Amazon Forest', M.S. Thesis. State University of New York at Albany, 121 pp.

Stull, R. B.: 1988, *An Introduction to Boundary Layer Meteorology*, Kluwer Academic Publishers, Boston, 666 pp.

Wexler, H.: 1961, 'A Boundary Layer Interpretation of the Low Level Jet', *Tellus* **13**, 368–378.

Wippermann, F.: 1973, 'Numerical Study on the Effects Controlling the Low-Level Jet', *Beiträge zur Physik der Atmosphäre* **46**, 137–154.

Yamada, T. and Mellor, G.: 1975, 'A Simulation of the Wangara Atmospheric Boundary Layer Data', *J. Atm. Sci.* **32**, 2309–2329.

Zhang, D. and Anthes, R. A.: 1982, 'A High Resolution Model of the Planetary Boundary Layer – Sensitivity Tests and Comparisons with the SESAME-79 Data', *J. Appl. Meteorrol.* **21**, 1594–1609.